Feedback control of subcritical Turing instability with zero mode

A. A. Golovin,[1,*] Y. Kanevsky,[2] and A. A. Nepomnyashchy[2]
[1]*Department of Engineering Sciences and Applied Mathematics, Northwestern University, Evanston, Illinois 60208, USA*
[2]*Department of Mathematics and Minerva Center for Physics of Complex Systems, Technion-Israel Institute of Technology, Haifa 32000, Israel*

(Received 10 July 2008; revised manuscript received 11 March 2009; published 24 April 2009)

A global feedback control of a system that exhibits a subcritical monotonic instability at a nonzero wave number (short-wave or Turing instability) in the presence of a zero mode is investigated using a Ginzburg-Landau equation coupled to an equation for the zero mode. This system is studied analytically and numerically. It is shown that feedback control, based on measuring the maximum of the pattern amplitude over the domain, can stabilize the system and lead to the formation of localized unipulse stationary states or traveling solitary waves. It is found that the unipulse traveling structures result from an instability of the stationary unipulse structures when one of the parameters characterizing the coupling between the periodic pattern and the zero mode exceeds a critical value that is determined by the zero mode damping coefficient.

DOI: 10.1103/PhysRevE.79.046218 PACS number(s): 89.75.Kd, 47.54.−r

I. INTRODUCTION

An important feature of pattern-forming systems is that near the instability threshold systems of different physical nature can be described by the same generic equations. For systems exhibiting Turing instability such equation is the real Ginzburg-Landau equation [1,2]. Systems exhibiting Hopf bifurcation, near threshold, are described by a complex Ginzburg-Landau equation [1,3].

However, there exists a large class of pattern-forming systems where a single Ginzburg-Landau equation is not sufficient for the description of the onset of pattern formation. That happens in the presence of a slowly evolving large-scale mode not enslaved to the unstable short-scale mode. In that case, an additional equation is needed for the description of the large-scale mode evolution. Typically, the origin of such long-scale mode is a symmetry of the system or a conservation law [4–8]. Physical examples include Marangoni convection in a liquid layer with deformable interface heated from below [9,10], instabilities in multimode lasers [11], nonlinear dynamics of sand banks and sand waves [12], Asaro-Tiller-Grinfeld instability of an epitaxial solid film in the presence of wetting interactions with the substrate [13], and many others (see [7]).

In the present paper, we consider systems subjected to a short-wave *monotonic* (Turing) instability and characterized by the conservation of a certain "mass" variable [7,9,10,13]. The generic system of amplitude equations is as follows:

$$A_t = A + A_{xx} - \lambda|A|^2 A + AB,$$

$$B_t = mB_{xx} + w(|A|^2)_{xx}, \tag{1}$$

where A is a complex amplitude of the unstable short-wave monotonic (Turing) mode and B is the amplitude of the zero mode associated with the conservation of mass. Here $m>0$, while w can be of either sign. Note that all the coefficients in Eq. (1) are real.

In a contradistinction to previous works on that subject, we consider here the case where the short-wave instability is subcritical, i.e., $\lambda=-1$ and $1-w/m>0$ in Eq. (1). One could assume that in that case the weakly nonlinear amplitude Eq. (1) is of no use, because the solutions bifurcating subcritically are unstable, and a blow-up is unavoidable [recall that the coefficients in Eq. (1) are real, therefore the dispersion mechanism of stabilization [11,14] does not work]. However, these solutions can be stabilized by means of a *feedback control*. That stabilization can be considered as a tool for the numerical investigation of the set of bifurcating solutions in the subcritical region of parameters.

Recall that feedback control of nonlinear dynamics in pattern-forming systems has been attracting large attention [15,16]. It was shown that it could be successfully applied to manipulate various physical processes such as Rayleigh-Benard and Marangoni convection [17–22], contact line instability in liquid films [23,24], shear flows [25–27], pattern formation in reaction-diffusion systems, excitable media [28–32] and catalytic reactions [33–35], patterns in nonlinear optics [36,37], instabilities in crystal growth [38,39], etc. The effect of feedback control on different systems near pattern formation threshold can be analyzed within the framework of the generic equations. For example, feedback control of wave dynamics governed by a complex Ginzburg-Landau equation was investigated in [40–44].

In the case of a subcritical instability, the feedback control can prevent the formation of large-amplitude structures and keep the dynamics of the system in a weakly nonlinear regime. In this case the system evolution can be described by amplitude equations with additional control terms. A typical feature in such subcritically unstable systems under feedback control is the formation of spatially localized structures, either stationary or oscillatory.

The choice of the control's type is determined by several circumstances. A linear control can successfully shift the threshold of the primary linear instability, but it is not efficient against the subcritical instabilities. A local control, when applied to extended systems, typically needs a large number of actuators. In the present paper, we apply a nonlinear control that affects only the *linear growth rate* of the

*Deceased.

primary instability. This way of control can be achieved by changing the global parameters of the system. For instance, in the case of a morphological instability of the solidification front it is implemented by changing the sample velocity and applied temperature gradient [39], in the case of a Marangoni instability it is sufficient to change the applied heat flux, etc. In order to avoid the blow-up that can develop in any spatial point, it is natural to measure and to control the maximum value of a characteristic variable (i.e., front deformation in the case of a morphological instability) over the whole region. Near the instability threshold, the deviation of that variable from its undisturbed value will be proportional to $\max_x|A|$. The simplest way of control that we consider here is making the deviation of the growth rate proportional to that quantity. In that case, we arrive to the following generic system of amplitude equations under global feedback control:

$$A_t = (1 - p \max_x |A|)A + A_{xx} + |A|^2 A + AB,$$

$$B_t = mB_{xx} + w|A|^2_{xx}. \tag{2}$$

Here p is the parameter characterizing the control strength. As noted above, this way of control can be implemented by changing the global parameters of the system. It has been shown formerly that it is efficient for arresting a localized blow-up in a number of pattern-formation problems, including the Sivashinsky equation [39], the Ginzburg-Landau equation with real [45] and complex [46] coefficients, as well as for controlling patterns described by the generalized Swift-Hohenberg equation [47].

The rest of the paper is structured as follows. We start with the description of numerical simulations of Eq. (2) that confirms the expected suppression of blow-up and reveals an unexpected phenomenon, the development of traveling wave solutions moving with velocity that strongly depends on the length of the computational region. Then we give a theoretical explanation of that phenomenon. We consider stationary solutions of system (2) in the form of spatially localized unipulse and multipulse structures, and discuss their stability. Then we consider traveling wave solutions and show that a localized traveling pulse bifurcates from the stationary localized state when the coupling parameter w exceeds a certain threshold. The dependence of the wave velocity on the spatial period is determined by means of a bifurcation analysis. In the last section, we present results of some additional numerical simulations that describe the effect of feedback delay.

II. NUMERICAL SIMULATIONS

The numerical simulations of Eq. (2) supplemented by periodic boundary conditions with a large period L have been performed using a pseudospectral code with time integration in Fourier space, Crank-Nicholson scheme for the linear operator and Adams-Bashforth scheme for the nonlinear one.

A characteristic feature of the system with the zero mode is the possibility of a shift $B(x) \to B(x) + \text{const}$ which leads to a shift of the linear growth rate for the short-wave mode A and hence can be reduced to a certain renormalization of the coefficients in the system of the amplitude equations. Therefore, it is sufficient to find solutions where the variable $B(x)$ is normalized in such a way that its averaged value over the whole domain is equal to zero,

$$\langle B(x) \rangle = \frac{1}{L} \int_{-L/2}^{L/2} B(x) dx = 0. \tag{3}$$

A. Stationary patterns

Direct numerical simulations of system (2) reveal two kinds of stationary solutions: (i) solutions with the period equal to L (unipulse solutions) and (ii) periodic solution with the period smaller than L (multipulse solutions). All the stationary solutions characterized by the constant values of the phase $\arg(A)$, and $|A|$ is not equal to zero in any points. The multipulse solutions are obtained only with perfectly periodic initial conditions, for example, for $L=160\pi$, $m=1.0$, $w=0.2$, $p=5.0$ a solution consisting of eight pulses is obtained (see Fig. 1). For the same parameters the unipulse solutions are obtained by using small-amplitude random initial conditions (see Fig. 2). In the case of a superposition of periodic and random component in initial conditions, a multipulse state is developed, but finally the most "strong" pulse starts to grow while other pulses are suppressed. A similar competition of pulses under the action of a global feedback control was formerly observed for a pure short-wave oscillatory instability [46].

B. Unipulse traveling wave solutions

Numerical simulations of system (2) show that the stationary solutions are stable only for $w < w_c$, where w_c depends on m and the period L. For $w > w_c$, a transition to either a traveling wave moving to the right,

$$A(x,t) = A_r(X_r), \quad B(x,t) = B_r(X_r), \quad X_r = x - ct, \quad c > 0, \tag{4}$$

or a traveling wave moving to the left,

$$A(x,t) = A_l(X_l), \quad B(x,t) = B_l(X_l), \quad X_l = x + ct, \quad c > 0, \tag{5}$$

is observed. Example of this instability is shown in Fig. 3.

Due to the symmetry of the problem, these two solutions are obtained from each other by reflection $x \to -x$, and their properties are equivalent. Figure 4 shows $c(w)$ for unipulse solutions at two different values of the control parameter p obtained from numerical simulations of system (2). One can see that while the threshold value w_c is the same for both values of p, the velocity of the unipulse traveling wave depends on p: the larger the control parameter, the smaller the velocity. The threshold value w_c weakly depends on the length of the computational region L (see Fig. 5). Near the threshold, the pulse velocity $c(w)$ tends to zero like $c \sim \sqrt{w - w_c}$, i.e., $c^2(w)$ is a linear function of w. Surprisingly, the derivative $dc^2(w)/dw$ in the point $w=w_c$ strongly depends on L. For instance, for $p=2.0$, $m=1.0$ the numerical value of the quantity $dc^2(w)/dw$ in the point $w=w_c$ obtained by the interpolation of numerical data is 0.049 for $L=40\pi$, and 0.0922 for $L=20\pi$.

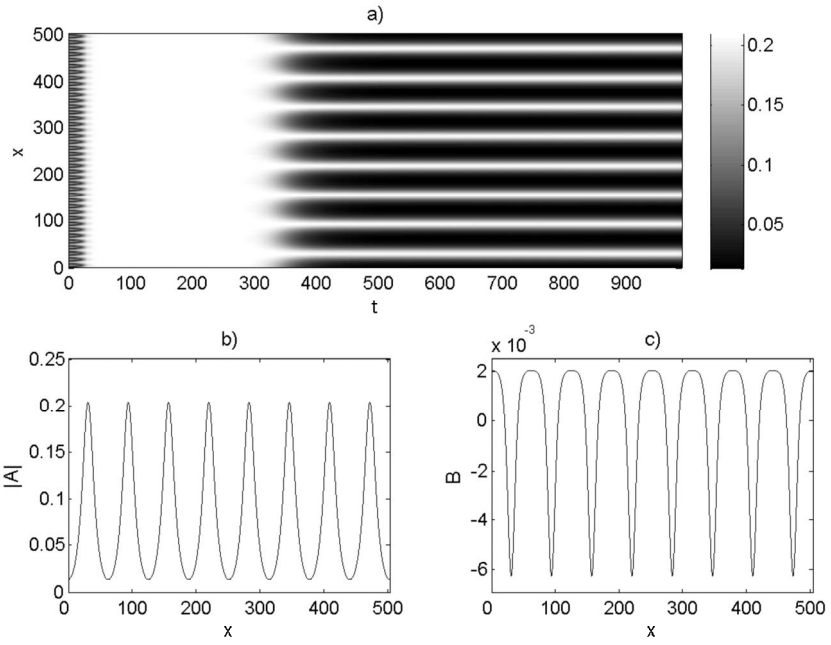

FIG. 1. Stationary multipulse solution of Eq. (2) described by Eqs. (13)–(15). (a) Formation of the multipulse solution from periodic initial conditions (spatiotemporal diagram, $|A|$ is shown); (b) $|A(x)|$; (c) $B(x)$; $w=0.2$, $p=5.0$, $m=1.0$, and $L=160\pi$.

C. Multipulse versus unipulse traveling structures

Here we investigate numerically the competition between traveling multipulse periodic structure and a single localized traveling pulse. Figure 6(a) shows the formation of a traveling multipulse structure starting from periodic initial conditions. Unless perturbed, this pattern persists indefinitely.

Figure 6(b) shows the spatiotemporal dynamics of this system when the computations start from the traveling multipulse solution shown in Fig. 6(a) perturbed by small-amplitude random noise. One can see the formation of a single localized traveling pulse. Thus we conclude that the traveling multipulse structure is unstable with respect to the formation of a single traveling pulse.

III. ANALYTICAL SOLUTIONS

A. Stationary patterns

In the present section we consider stationary solutions of problem (2). Because the structures obtained in numerics are characterized by a constant value of the phase, we fix that value equal to zero and arrive to the following system of equations for real variables A and B:

$$A_{xx} + (1 - p \max_x A)A + A^3 + AB = 0, \tag{6}$$

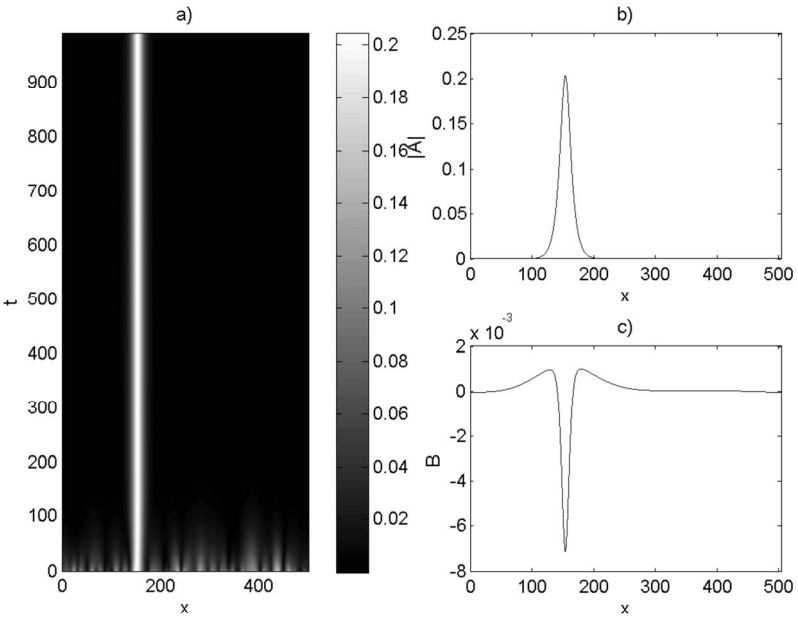

FIG. 2. Stationary unipulse solution of Eq. (2) described by Eqs. (19) and (20). (a) Formation of the unipulse solution from random initial conditions (spatiotemporal diagram, $|A|$ is shown); (b) $|A(x)|$; (c) $B(x)$; $w=0.2$, $p=5.0$, $m=1.0$, and $L=160\pi$.

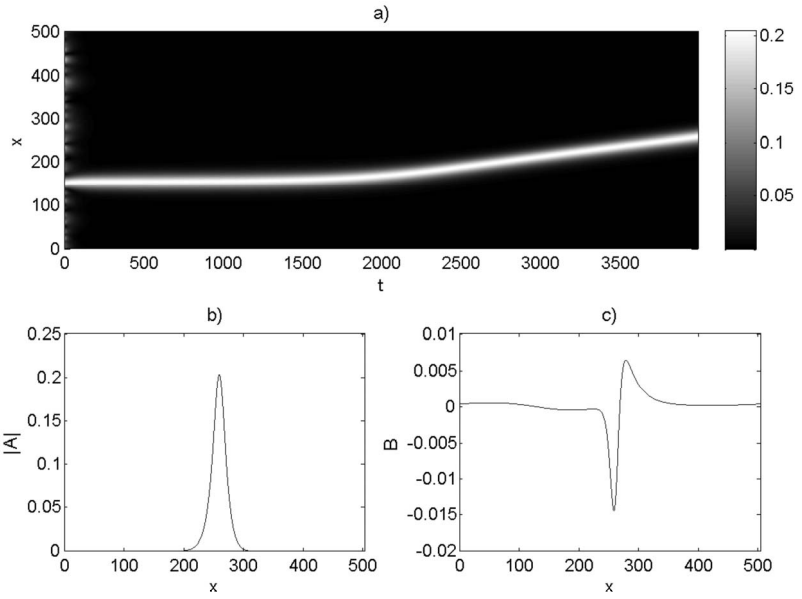

FIG. 3. Traveling unipulse solution of Eq. (2). (a) Formation of the traveling solution resulting from an instability of a stationary unipulse solution (spatiotemporal diagram, $|A|$ is shown, random initial conditions); (b) $|A(x)|$ and (c) $B(x)$ at a particular moment of time; $p=5.0$; $w=0.5$, $m=1.0$, and $L=160\pi$.

$$mB_{xx} + w(A^2)_{xx} = 0. \tag{7}$$

Only sign-preserving (positive) solutions corresponding to structures observed in numerical simulations are discussed below. Recall that

$$\langle B(x)\rangle = 0, \tag{8}$$

$m>0$, while w may have either sign.

The bounded solution $B(x)$ of Eq. (7) satisfying condition (8) is

$$B(x) = \left(-\frac{w}{m}\right)(|A(x)|^2 - \langle A^2\rangle), \tag{9}$$

which leads to the following closed equation for the amplitude $A(x)$:

$$A_{xx} - \alpha A + \beta A^3 = 0, \tag{10}$$

where

$$\alpha = -1 + p \max_x |A| + \frac{w}{m}\langle A^2\rangle, \quad \beta = 1 - \frac{w}{m}. \tag{11}$$

The coefficient α determines the effective linear decay rate of the short-wave amplitude in the presence of the global control and the zero mode, while β is the Landau coefficient renormalized due to the action of the zero mode.

Integration of Eq. (10) gives the relation

$$\frac{A_x^2}{2} - \frac{\alpha A^2}{2} + \frac{\beta A^4}{4} = E = \text{const}. \tag{12}$$

The positive solutions exist when $\alpha>0$, $\beta>0$, $-\alpha^2/4\beta < E < 0$, and they can be presented in terms of Jacobi elliptic functions,

$$A(x) = A_m \,\mathrm{dn}\left[A_m\sqrt{\frac{\beta}{2}}(x-x_0); s\right], \tag{13}$$

where A_m is connected with the parameter α by the relation $\alpha=(2-s^2)\beta A_m^2/2$, and s is the modulus of the elliptic func-

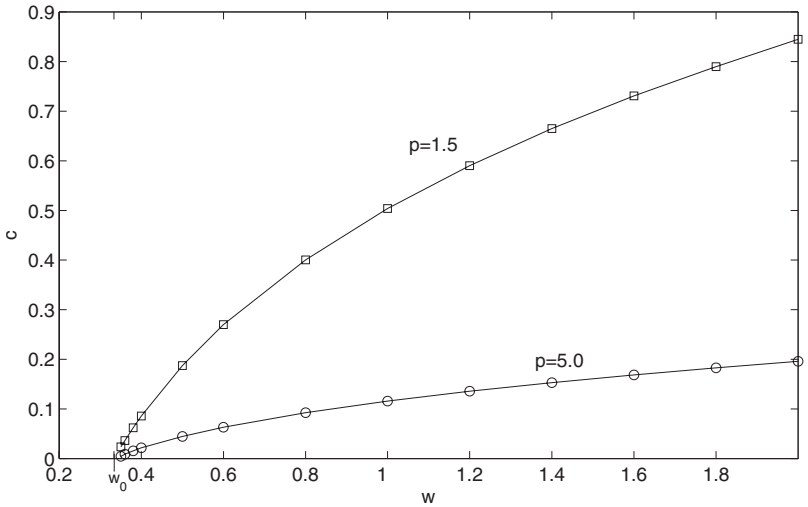

FIG. 4. Bifurcation diagram showing the dependence of the traveling wave speed as a function of the coupling parameter, $c(w)$, for $L=160\pi$, $m=1.0$, and two different values of the control parameter p; w_0 is threshold value (51) predicted by the theory in the limit $L\gg 1$.

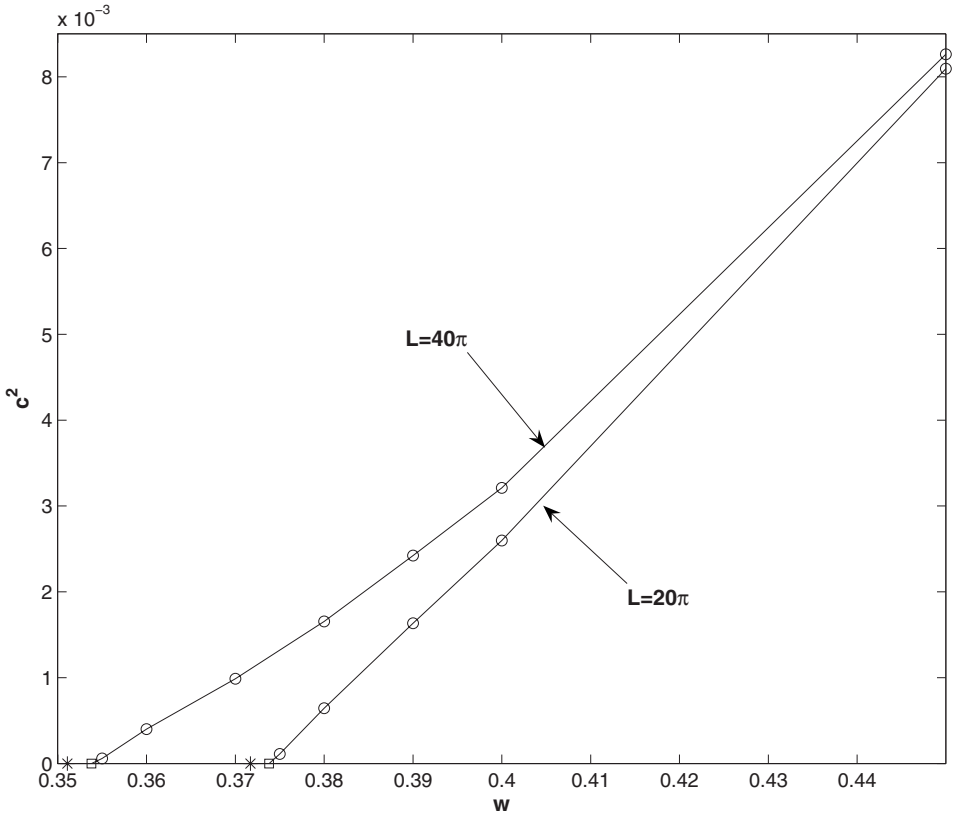

FIG. 5. Bifurcation diagram showing the dependence of the traveling wave speed as a function of the coupling parameter, $c^2(w)$, for $p=2.0$, $m=1.0$, and two different values of the domain length L. The circles denote the results of direct numerical simulation of system (2). The squares denote the extrapolated threshold values w_c, $w_c \approx 0.374$ for $L=20\pi$ and $w_c \approx 0.354$ for $L=40\pi$. The theoretical predictions w_0 according to Eq. (49) are marked by stars, $w_0=0.372$ for $L=20\pi$ and $w_0=0.351$ for $L=40\pi$.

tion. With $\langle A^2 \rangle = A_m^2 E(s)/K(s)$ [where $K(s)$ and $E(s)$ are the complete elliptic integrals of the first and the second kind, respectively] Eq. (11) gives the following equation that determines the amplitude A_m as a function of s:

$$\left[\frac{1}{2}\left(1-\frac{w}{m}\right)(2-s^2)+\frac{w}{2m}\frac{E(s)}{K(s)}\right]A_m^2 - pA_m + 1 = 0. \quad (14)$$

The period of solution (13) is

$$L = \frac{2\sqrt{2}K(s)}{A_m\sqrt{1-w/m}}. \quad (15)$$

Recall that an eight-pulse numerical solution is obtained for $m=1.0$, $w=0.2$, $p=5.0$, and $L=160\pi$; see Fig. 1. In order to compare the analytical and numerical results, we calculate analytical solution (13) and Eq. (9) for $w=0.2$, $p=5.0$, and $L=20\pi$, which describes an eight-pulse structure within a domain with the length $L=160\pi$. We find that three digits of the numerical solution coincide with those of the analytical

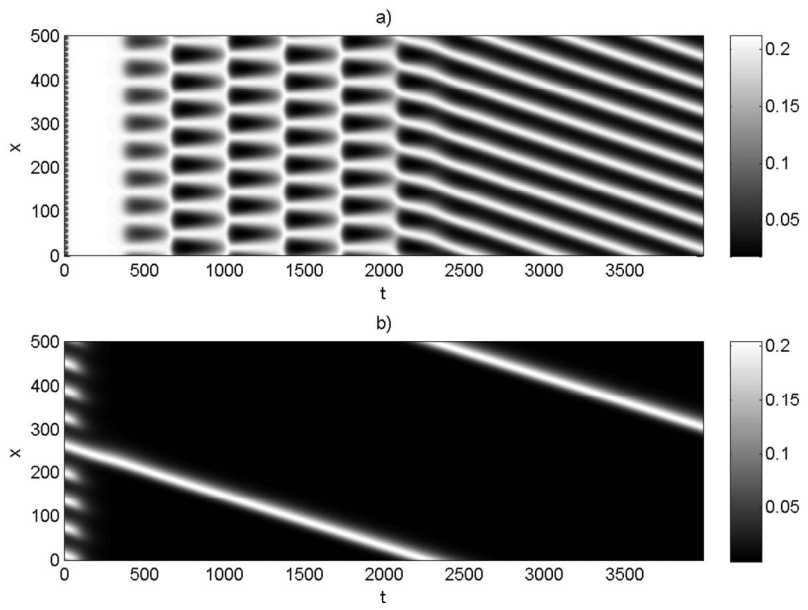

FIG. 6. (a) Formation of a traveling multipulse structure starting from periodic initial condition. (b) Formation of a single traveling pulse resulting from the instability of the traveling multipulse structure with respect to small-amplitude random perturbation; $p=5.0$, $w=1.0$, $m=1.0$, and $L=160\pi$.

solution, hence both solutions would be undistinguishable in plots (b) and (c) in Fig. 1.

In the limit $s \to 1$ ($E \to 0$) the periodic solution tends to a localized solution such that both $A(x)$ and $B(x)$ tend to zero at infinity. In this case

$$B(x) = -\frac{w}{m}A^2, \tag{16}$$

and the function $A(x)$ satisfies the equation

$$A_{xx} + (1 - p \max_x A)A + \left(1 - \frac{w}{m}\right)A^3 = 0. \tag{17}$$

Two nonzero localized solutions of Eq. (17), $[A_\pm(x), B_\pm(x)]$, exist in the following interval of the coupling parameter w:

$$w_{\min} = m(2 - p^2)/2 \le w < m, \tag{18}$$

and are given by

$$A_\pm(x) = a_\pm \cosh^{-1}[k_\pm(x - x_0)],$$

$$B_\pm(x) = -\frac{w}{m}a^2 \cosh^{-2}[k_\pm(x - x_0)], \tag{19}$$

where

$$a_\pm = \frac{p \pm \sqrt{p^2 - 2(1 - w/m)}}{1 - w/m}, \quad k_\pm = \frac{1}{\sqrt{2}}\sqrt{1 - \frac{w}{m}}a_\pm. \tag{20}$$

The localized solutions (19) and (20) describe rather well the shape of a unipulse solution obtained numerically in a sufficiently long region. We have compared the unipulse solution shown in Fig. 2, which has been obtained in a domain of the length $L = 160\pi$, with the limit solution (19) with $A = A_-$. Three digits of both results coincide, therefore, the analytical solution is undistinguishable from the numerical result shown in Fig. 2(b).

B. Stability of localized pulses

In the numerical simulations, only solutions $[A_-(x), B_-(x)]$ are observed. It is natural to assume that solutions $[A_+(x), B_+(x)]$ are unstable. In the present section, we check this assumption near the bifurcation point

$$p = p_* = \sqrt{2\beta}, \quad \beta = 1 - \frac{w}{m}, \tag{21}$$

where two branches of stationary solutions are born due to a saddle-node bifurcation.

Let us parametrize the family of solutions (19) and (20) using parameter k. Take $x_0 = 0$ (obviously, the stability does not depend on x_0). Both branches of solutions can be written as

$$A = a \cosh^{-1}(kx), \quad B = -\frac{w}{m}A^2, \tag{22}$$

where

$$a = \sqrt{\frac{2}{\beta}}k, \quad p = \sqrt{\frac{\beta}{2}}\frac{k^2 + 1}{k}. \tag{23}$$

Solutions with $k < 1$ correspond to the lower branch, while solutions with $k > 1$ correspond to the upper branch.

The time evolution of real disturbances $(\tilde{A}^r, \tilde{B})$ on the background of Eq. (22) is governed by the following system of functional-differential equations:

$$\tilde{A}^r_t = \tilde{A}^r_{xx} + (-k^2 + 3A^2 + B)\tilde{A}^r + A\tilde{B} - pA\tilde{A}^r(0,t), \tag{24}$$

$$\tilde{B}_t = m\tilde{B}_{xx} + 2w(A\tilde{A}^r)_{xx}. \tag{25}$$

Defining $z = kx$ and assuming $\tilde{A}^r = u(z)\exp(\sigma t)$, $\tilde{B} = v(z)\exp(\sigma t)$, we obtain the following system:

$$u_{zz}(z) + \left[-1 - \frac{\sigma}{k^2} + \frac{2(2+\beta)}{\beta \cosh^2 z}\right]u(z) + \frac{\sqrt{2}}{k\sqrt{\beta}}\frac{v(z)}{\cosh z} = \left(1 + \frac{1}{k^2}\right)\frac{u(0)}{\cosh z}, \tag{26}$$

$$v_{zz}(z) + \frac{2w}{m}\sqrt{\frac{2}{\beta}}k\left[\frac{u(z)}{\cosh z}\right]_{zz} - \frac{\sigma}{mk^2}v(z) = 0. \tag{27}$$

Due to the symmetry of the problem, both components of the eigenfunction $[u(z), v(z)]$ are either even or odd. For odd eigenfunctions, $u(0) = 0$, while for even ones generally $u(0) \neq 0$. In the present section, we consider even disturbances and normalize the solution of the problem [Eqs. (26) and (27)] by the condition

$$u(0) = 1. \tag{28}$$

For $k = 1$, i.e., in the point of the saddle-node bifurcation leading to the creation of two branches of solutions for $p > \sqrt{2\beta}$, the problem [Eqs. (26) and (27)] has the following exact solution:

$$\sigma = 0, \quad u = u_0 = \frac{1}{\cosh z} - z \sinh z \cosh^2 z,$$

$$v = v_0 = -\frac{2w}{m}\sqrt{\frac{2}{\beta}}\frac{u_0}{\cosh z}. \tag{29}$$

Near that point, we apply the expansion

$$\frac{1}{k^2} = 1 + \epsilon, \quad \sigma = \epsilon\sigma_1 + \ldots, \quad u = u_0 + \epsilon u_1 + \ldots,$$

$$v = v_0 + \epsilon v_1 + \ldots.$$

Note that $k = 1 - \epsilon/2 + \ldots$, hence $\epsilon > 0$ ($\epsilon < 0$) corresponds to the lower (upper) branch of solutions.

At the first order in ϵ, the following system is obtained:

$$(u_1)_{zz} + \left[-1 + \frac{2(2+\beta)}{\beta \cosh^2 z}\right]u_1 + \sqrt{\frac{2}{\beta}}\frac{v_1}{\cosh z} = \frac{1}{\cosh z} + \sigma_1 u_0 - \frac{1}{2}\sqrt{\frac{2}{\beta}}\frac{v_0}{\cosh z}, \tag{30}$$

$$(v_1)_{zz} + \frac{2w}{m}\sqrt{\frac{2}{\beta}}\left(\frac{u_1}{\cosh z}\right)_{zz} = \frac{\sigma_1}{m}v_0 + \frac{w}{m}\sqrt{\frac{2}{\beta}}\left(\frac{u_0}{\cosh z}\right)_{zz}. \tag{31}$$

Eliminating v_1, we find

$$(u_1)_{zz} + \left(-1 + \frac{6}{\cosh^2 z}\right)u_1 = \frac{1}{\cosh z} + \sigma_1\left[u_0 + \frac{2}{\beta}\frac{w}{m^2}\frac{z\sinh z}{\cosh^2 z}\right],$$

$$|u_1| < \infty, \quad z \to \pm\infty. \tag{32}$$

Problem (32) is solvable when its right-hand side is orthogonal to the solution of the homogeneous problem, which is u_0, hence

$$\sigma_1 = -\frac{\int_{-\infty}^{\infty} u_0 \cosh^{-1}(z)dz}{\int_{-\infty}^{\infty} u_0\left[u_0 + \frac{2}{\beta}\frac{w}{m^2}\frac{z\sinh z}{\cosh^2 z}\right]dz}. \tag{33}$$

Calculating the integral, we find

$$\sigma_1 = -\frac{18}{(12+\pi^2) - 2(\pi^2-6)w/(\beta m^2)}. \tag{34}$$

One can see that if

$$w < w_* = \frac{m^2}{m + 2(\pi^2-6)/(\pi^2+12)}, \tag{35}$$

then $\sigma_1 < 0$. This means that in region (35) the upper branch (that with $\epsilon < 0$) is unstable, while the lower branch (that with $\epsilon > 0$) is stable with respect to *even* real disturbances. In the contradistinction to the case where the zero mode is absent, for $w > w_*$ the lower branch becomes unstable, and the upper branch becomes stable with respect to that kind of disturbances. However, in Sec. III C it will be shown that the stationary solutions become unstable with respect to *odd* disturbances leading to the development of traveling waves at the value $w = w_0 = m^2/(m+2) < w_*$.

C. Traveling waves

In the present section, we find the transition threshold and analyze the bifurcation of the traveling wave solutions $A = A(X)$, $B = B(X)$, and $X = x - ct$, which satisfy the system of equations

$$A_{XX} + cA_X + A(1 - p\max_X|A|) + A^3 + AB = 0, \tag{36}$$

$$mB_{XX} + cB_X + w(A^2)_{XX} = 0, \tag{37}$$

with periodicity conditions

$$A(X+L) = A(X), \quad B(X+L) = B(X), \tag{38}$$

and the condition of zero mean value of B:

$$\langle B\rangle = \frac{1}{L}\int_{-L/2}^{L/2} B(X)dX = 0. \tag{39}$$

1. Mechanism of traveling wave propagation

The mechanism of a traveling wave propagation is similar to that known for an activator-inhibitor system [48], where the component A plays the role of an activator and the quantity $-B$ corresponds to the concentration of an inhibitor. The coupling between the components is different from that used in the standard FitzHugh-Nagumo (FHN) model. Nevertheless, the distribution of the inhibitor $-B$ in a moving pulse is similar to that in a FHN model (see [49]): the component B is positive in the front part of the pulse and negative in the back part of the pulse. Therefore, the growth of the component A is enhanced in the front part and suppressed in the back part, which leads to the effective motion of the pulse as the whole. The shape of the profile of $B(x)$ can be roughly understood from Eq. (37) in the limit where the diffusion term mB_{XX} is small in comparison with cB_X: in that case it holds that $B \sim (-w/c)(A^2)_X$.

2. Transition's threshold

Let us define the operator

$$\partial_X^{-1}B = \int_0^X B(y)dy - \langle\int_0^X B(y)dy\rangle, \tag{40}$$

and rewrite Eq. (37) in the form

$$B = -\frac{w}{m}(A^2 - \langle A^2\rangle) - \frac{c}{m}\partial_X^{-1}B. \tag{41}$$

Substituting Eq. (41) into Eq. (36), we obtain

$$A_{XX} + A\left(1 - p\max_X A + \frac{w}{m}\langle A^2\rangle\right) + \left(1 - \frac{w}{m}\right)A^3 = c\left(-A_X + \frac{1}{m}A\partial_X^{-1}B\right). \tag{42}$$

Near the bifurcation point, we expect the following expansions:

$$A = A_0 + \epsilon A_1 + \epsilon^2 A_2 + \ldots, \quad B = B_0 + \epsilon B_1 + \epsilon^2 B^2 + \ldots,$$
$$c = \epsilon c_1 + \ldots, \quad w = w_0 + \epsilon w_2 + \ldots. \tag{43}$$

The zeroth order terms A_0 and B_0 correspond to the stationary solutions (13) and (9). Let us choose the constant $x_0 = 0$ so that these functions are even. Then the correction A_1 is an odd function satisfying the following equation:

$$(A_1)_{XX} + A_1\left(1 - p\max_X A_0 + \frac{w_0}{m}\langle A_0^2\rangle\right) + 3\left(1 - \frac{w_0}{m}\right)A_0^2A_1 = c_1\left[-(A_0)_X + \frac{1}{m}A_0\partial_X^{-1}B_0\right], \tag{44}$$

$$A_1(X+L) = A_1(X) \tag{45}$$

[note that the addition of an odd function A_1 does not change the maximum value of $A_0 + \epsilon A_1$ in the order $O(\epsilon)$]. The self-

adjoint homogeneous problem corresponding to the linear operator on the left-hand side of Eq. (44) has a solution $A_1^h(X)=(A_0)_X(X)$. The solvability condition for the inhomogeneous problem [Eqs. (44) and (45)] is the condition of the orthogonality of the right-hand side to that solution,

$$-\langle[(A_0)_X]^2\rangle+\frac{1}{m}\langle(A_0)_X A_0\partial_X^{-1}B_0\rangle=0. \tag{46}$$

Taking into account that $(A_0)_X A_0=-(m/2w_0)(B_0)_X$ and integrating the second integral in Eq. (46) by parts, we find

$$-\langle[(A_0)_X]^2\rangle+\frac{1}{2w_0}\langle B_0^2\rangle=0. \tag{47}$$

Substituting

$$B_0=-\frac{w_0}{m}(A_0^2-\langle A_0^2\rangle)$$

[according to Eq. (9)], we obtain the solvability condition in the form

$$-\langle[(A_0)_X]^2\rangle+\frac{w_0}{2m^2}[\langle A_0^4\rangle-(\langle A_0^2\rangle)^2]=0. \tag{48}$$

Substituting solution (13) for A_0, we arrive at the following expression for the threshold of the transition from the stationary to traveling-wave solutions:

$$w_0=\frac{m^2}{m+f(s)}, \tag{49}$$

where

$$f(s)=\frac{-(1-s^2)+2(2-s^2)E(s)/K(s)-3[E(s)/K(s)]^2}{-2(1-s^2)+(2-s^2)E(s)/K(s)}. \tag{50}$$

In the limit of the localized solution ($s\to 1$) one finds

$$w_0=\frac{m^2}{m+2}, \tag{51}$$

while in the limit of small-amplitude waves ($s\to 0$),

$$w_0=\frac{m^2}{m+1}. \tag{52}$$

Note that the instability threshold does not depend on the control parameter p but only on the zero-mode damping coefficient m. Equations (49) and (51) are well confirmed by our numerical simulations (see Figs. 4 and 5).

3. Bifurcation analysis

As we mentioned in Sec. II, the bifurcation of traveling wave solutions reveals a surprising dependence of the bifurcation parameter $[dc^2(w)/dw]|_{w=w_0}$ on the period L. To explain that unusual phenomenon, we perform the nonlinear analysis of the bifurcation in the limit $L\gg 1$, which corresponds to the numerical simulations. In this case elliptic function (13) can be approximated by localized solution (19).

For small c, iterating relation (41), we find

$$B=-\frac{w}{m}\left[1-\frac{c}{m}\partial_X^{-1}+\left(\frac{c}{m}\right)^2\partial_X^{-2}-\left(\frac{c}{m}\right)^3\partial_X^{-3}+O(c^4)\right]\times(A^2-\langle A^2\rangle). \tag{53}$$

Substituting Eq. (53) into Eq. (36), we obtain a closed integrodifferential equation for $A(X)$:

$$A_{XX}+cA_X+A(1-p\max_X A)+A^3-\frac{w}{m}A\left[1-\frac{c}{m}\partial_X^{-1}+\left(\frac{c}{m}\right)^2\partial_X^{-2}-\left(\frac{c}{m}\right)^3\partial_X^{-3}+O(c^4)\right]\times(A^2-\langle A^2\rangle). \tag{54}$$

We search the solution in the interval $-L/2\le X\le L/2$.

Substitute expansion (43) into Eq. (54) and equate the terms of the same order in ϵ. At the zeroth order, we obtain the equation which is identical to that obtained above for the stationary solution:

$$(A_0)_{XX}+A_0(1-p\max_X A_0)+(A_0)^3-\frac{w_0}{m}A_0(A_0^2-\langle A_0^2\rangle)=0. \tag{55}$$

In the limit of large L the solution $A_0(X)$ can be approximated by the localized solution [we choose the origin is such a way that $A_0(X)$ is an even function]:

$$A_0(X)=a\cosh^{-1}kX, \tag{56}$$

where

$$a=\left[p-\sqrt{p^2-2\left(1-\frac{w_0}{m}\right)}\right]\Big/\left(1-\frac{w_0}{m}\right),$$

$$k^2=\frac{1}{2}\left(1-\frac{w_0}{m}\right)a^2.$$

At the first order, as shown in the previous subsection, the solution is governed by the equation

$$\hat{L}A_1=(A_1)_{XX}+A_1(1-pa)+3\left(1-\frac{w_0}{m}\right)A_0^2A_1=c_1\left[-(A_0)_X-\frac{w_0}{m^2}A_0\partial_X^{-1}(A_0^2-\langle A_0^2\rangle)\right]. \tag{57}$$

The solvability condition for Eq. (57) is the orthogonality of the right-hand side to $(A_0)_X$ [the integral is calculated on the interval $(-L/2,L/2)$]. In the limit of large L,

$$\partial_X^{-1}(A_0^2-\langle A_0^2\rangle)=\frac{a^2}{k}\left(\tanh(kX)-\frac{2X}{L}\right). \tag{58}$$

Because the function $(A_0)_X$ is exponentially small in the region $|X|\gg 1$, the behavior of all the functions is relevant only in the region $X=O(1)$. Finally, we obtain threshold value (51). In the bifurcation point, the right-hand side of Eq. (57) is $O(1/L)$, hence the solution $A_1=C(A_0)_X+O(1/L)$, which corresponds to the possibility of an arbitrary translation of the solution, due to the symmetry of the original problem. Here and below we shall select the solution with $C=0$, hence $A_1(X)=O(1/L)$ (note that

$$B_1(X) = \frac{c_1 w_0}{m^2}\partial_X^{-1}(A_0^2 - \langle A_0^2\rangle) = \frac{c_1 w_0 a^2}{m^2 k}\left(\tanh(kX) - \frac{2X}{L}\right)$$

is not small).

At the second order, the equation is as follows:

$$\hat{L}A_2 = pA_0(X)\max_X(A_2) + \frac{w_2}{m}A_0(A_0^2 - \langle A_0^2\rangle) + \frac{w_0 c_1^2}{m^3}A_0\partial_X^{-2}(A_0^2 - \langle A_0^2\rangle) - \frac{2w_0 A_0}{m}\langle A_0 A_2\rangle. \quad (59)$$

The function on the right-hand side is even; hence, the solvability condition is always satisfied. The solution can be presented in the form

$$A_2 = w_2 A_2^w + c_1^2 A_2^c,$$

where A_2^w and A_2^c are solutions of the following equations:

$$\hat{L}A_2^w = pA_0(X)\max_X(A_2^w) + \frac{1}{m}A_0(A_0^2 - \langle A_0^2\rangle) - \frac{2w_0 A_0}{m}\langle A_0 A_2^w\rangle, \quad (60)$$

$$\hat{L}A_2^c = pA_0(X)\max_X(A_2^c) + \frac{w_0}{m^3}A_0\partial_X^{-2}(A_0^2 - \langle A_0^2\rangle) - \frac{2w_0 A_0}{m}\langle A_0 A_2^c\rangle. \quad (61)$$

Note that

$$\partial_X^{-2}(A_0^2 - \langle A_0^2\rangle) = \frac{a^2}{k}\left(\frac{1}{k}\ln\cosh(kX) - \frac{x^2}{L} - \frac{L}{6}\right). \quad (62)$$

Thus, in the region $X=O(1)$ the corresponding term is $O(L)$. As noted above, the bifurcation equation is determined by the values of the functions in the region $X=O(1)$. In this region, the solutions in the leading order of L are as follows:

$$A_2^w = \frac{a^3}{2m(k^2-1)}\cosh^{-1} kX - \frac{a^3(1+k^2)}{4mk(k^2-1)}X\sinh kX\cosh^{-2} kX + O(1/L), \quad (63)$$

$$A_2^c = -\frac{w_0 a^3 L}{6m^3 k(k^2-1)}(\cosh^{-1} kX - kX\sinh kX\cosh^{-2} kX) + O(1). \quad (64)$$

At the third order, we obtain the following equation:

$$\hat{L}A_3 = -c_1(A_2)_X - \frac{w_2 c_1}{m^2}A_0\partial_X^{-1}(A_0^2 - \langle A_0^2\rangle) - \frac{w_0 c_1}{m^2}A_2\partial_X^{-1}(A_0^2 - \langle A_0^2\rangle) - \frac{2w_0 c_1}{m^2}A_0\partial_X^{-1}(A_0 A_2 - \langle A_0 A_2\rangle) - \frac{w_0 c_1^3}{m^4}A_0\partial_X^{-3}(A_0^2 - \langle A_0^2\rangle). \quad (65)$$

Substituting Eqs. (56), (63), and (64) into the solvability condition of Eq. (65), we obtain the bifurcation equation

$$c_1(w_2 I_w + c_1^2 I_c) = 0, \quad (66)$$

where

$$I_w = \langle A_{0X}A_{2X}^w\rangle + \frac{1}{m^2}\langle A_{0X}A_0\partial_X^{-1}(A_0^2 - \langle A_0^2\rangle)\rangle + \frac{w_0}{m^2}\langle A_{0X}A_2^w\partial_X^{-1}(A_0^2 - \langle A_0^2\rangle)\rangle + \frac{2w_0}{m^2}\langle A_{0X}A_0\partial_X^{-1}(A_0A_2^w - \langle A_0A_2^w\rangle)\rangle,$$

$$I_c = \langle A_{0X}A_{2X}^c\rangle + \frac{w_0}{m^2}\langle A_{0X}A_2^c\partial_X^{-1}(A_0^2 - \langle A_0^2\rangle)\rangle + \frac{2w_0}{m^2}\langle A_{0X}A_0\partial_X^{-1}(A_0A_2^c - \langle A_0A_2^c\rangle)\rangle + \frac{w_0}{m^4}\langle A_{0X}A_0\partial_X^{-3}(A_0^2 - \langle A_0^2\rangle)\rangle.$$

Using integration by parts, one finds that

$$I_w = \left\langle A_2^w\left[-A_{0XX} + \frac{w_0}{m^2}A_{0X}\partial_X^{-1}(A_0^2 - \langle A_0^2\rangle) - \frac{w_0}{m^2}A_0^3\right]\right\rangle - \frac{1}{m^2}\langle A_0^4\rangle + O(1/L^2).$$

Evaluation of this expression, which is done with the help of the relation

$$A_{0XX} + \frac{w_0}{m^2}A_{0X}\partial_X^{-1}(A_0^2 - \langle A_0^2\rangle) + \frac{w_0}{m^2}A_0^3 = O(1/L^2)$$

[for $X=O(1)$], gives

$$I_w = -\frac{a^4}{3w_0 kL} + O(1/L^2).$$

Similarly, I_c can be transformed to the following expression:

$$I_c = \frac{2w_0}{m^2}\langle A_2^c A_{0X}A_0\partial_X^{-1}(A_0^2 - \langle A_0^2\rangle)\rangle + \frac{w_0 a^2 L}{12m^4 k}\langle A_0^2\rangle + O(1/L).$$

Finally, we obtain

$$I_c = \frac{w_0 a^4}{6m^4 k^2} + O(1/L).$$

Using the obtained values of the coefficients I_w and I_c, we find that at the threshold point

$$\frac{dc^2(w)}{dw} = \frac{c_1^2}{w_2} = -\frac{I_w}{I_c} = \frac{2k(m+2)^2}{L}. \quad (67)$$

Note that this quantity tends to zero as $L\to\infty$.

The values of the quantity $dc^2(w)/dw$ obtained by interpolation of numerical data are rather close to those predicted

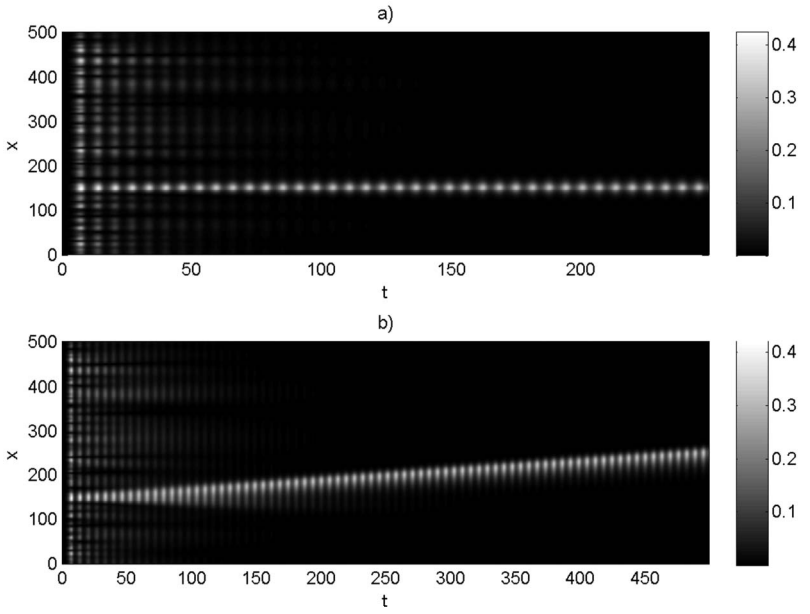

FIG. 7. (a) Formation of a unipulse oscillating solution with a stationary location; $p=5.0$; $w=0.2$, $m=1.0$, $L=160\pi$, and $\tau=1.5$. (b) Formation of a traveling oscillating solution; $p=5.0$, $w=2.0$, $m=1.0$, $L=160\pi$, and $\tau=1.5$.

by formula (67). For instance, for $p=2.0$, $m=1.0$, the theoretical values are 0.0456 and 0.0912 for $L=40\pi$ and $L=20\pi$, correspondingly, which are close to the numerical values 0.049 and 0.0922.

IV. EFFECT OF FEEDBACK DELAY

In systems with feedback control, there is usually a delay between the measurements and the application of the control action. In some cases, time-delayed feedback is applied intentionally as a part of the control method (see [50]). In other cases, the nonlocal feedback control is a feature of a natural system, specifically, it is characteristic for the brain activity [51]. In the present paper we consider the system evolution described by the following coupled equations:

$$A_t = (1 - p \max_x |A(t-\tau)|)A + A_{xx} + |A|^2 A + AB, \quad (68)$$

$$B_t = mB_{xx} + w|A|^2_{xx}. \quad (69)$$

Note that this kind of delay control was considered formerly for subcritical monotonic instability in the absence of a zero mode [45,47] and for a subcritical oscillatory instability [46].

We have performed numerical simulations for different values of the delay τ and the coupling parameter w. We have found that the behavior of both stationary and traveling unipulse solutions is similar. When the delay τ exceeds a certain threshold value the unipulse solutions exhibit oscillations. The onset of oscillations for $m=1.0$, $p=5.0$, and $L=160\pi$ occurs when $\tau \approx 1.464$ for $w=0.2$ and $\tau \approx 1.462$ for $w=2.0$. The amplitude of the oscillations grows with the increase in the delay. When the delay exceeds a second threshold value (for $m=1.0$, $p=5.0$, and $L=160\pi$ it is $\tau \approx 1.9576$ for $w=0.2$ and $\tau \approx 2.0003$ for $w=2.0$) the solution blows up. Thus, the behavior of both stationary and traveling unipulse solutions with the increase in the delay is similar to the behavior of a stationary localized solution of a real, controlled subcritical Ginzburg-Landau equation studied in [45]. Examples of oscillating unipulse solutions of system (68) are shown in Fig. 7. Figure 7(a) shows the formation of an oscillating unipulse solution whose location is stationary. With the increase in the coupling parameter w this solution loses stability with respect to the formation of a traveling, oscillating localized structure. The formation of this traveling, unipulse oscillating solution is shown in Fig. 7(b).

V. CONCLUSIONS

We have investigated the effect of feedback control on the dynamics of a subcritical Turing instability in a system with zero mode near the instability threshold within the framework of a system of two coupled equations (2): a Ginzburg-Landau equation with a feedback control term for the Turing mode coupled to an equation for the zero mode. The feedback control is based on measuring the maximum amplitude of the forming Turing pattern and adjusting the supercriticality of the system. We have demonstrated that the chosen feedback control can suppress the blow-up and can keep the system in the weakly nonlinear regime. As a result, a localized structure is formed, whose nature depends on the parameter characterizing the coupling between the Turing mode and the zero mode. For small enough values of the coupling parameter, the localized structure is stationary and it is similar to that forming in controlled subcritical systems studied in [45]. When the coupling parameter exceeds a critical value, which depends only on the damping coefficient of the zero mode, the stationary structure loses stability with respect to a traveling, spatially localized solution. The traveling speed increases with the increase in the coupling parameter and decreases with the increase in the control strength. The results of the linear stability analysis and the bifurcation analysis near the instability threshold are in good agreement with the numerical simulations. We have also studied the effect of the feedback delay. We have found that when the

delay exceeds a certain threshold the amplitude of the unipulse structures, both stationary and traveling ones, exhibit oscillations. The amplitude of these oscillations grows with the increase in the delay until the solution blows up when the delay exceeds a second threshold.

ACKNOWLEDGMENTS

A.A.G. acknowledges the support of the U.S. NSF under Grant No. DMS-0505878. A.A.N. acknowledges the support of the Israel Science Foundation under Grant No. 812/06.

[1] M. C. Cross and P. C. Hohenberg, Rev. Mod. Phys. **65**, 851 (1993).
[2] D. Walgraef, *Spatio-Temporal Pattern Formation: With Examples from Physics, Chemistry, and Materials Science* (Springer-Verlag, Berlin, 1997).
[3] I. S. Aranson and L. Kramer, Rev. Mod. Phys. **74**, 99 (2002).
[4] P. Coullet and S. Fauve, Phys. Rev. Lett. **55**, 2857 (1985).
[5] P. Coullet and G. Iooss, Phys. Rev. Lett. **64**, 866 (1990).
[6] P. C. Matthews and S. M. Cox, Phys. Rev. E **62**, R1473 (2000).
[7] P. C. Matthews and S. M. Cox, Nonlinearity **13**, 1293 (2000).
[8] S. M. Cox and P. C. Matthews, Physica D **175**, 196 (2003).
[9] A. A. Golovin, A. A. Nepomnyashchy, and L. M. Pismen, Phys. Fluids **6**, 34 (1994).
[10] A. A. Golovin, A. A. Nepomnyashchy, and L. M. Pismen, J. Fluid Mech. **341**, 317 (1997).
[11] D. Casini, G. D'Alessandro, and A. Politi, Phys. Rev. A **55**, 751 (1997).
[12] N. Komarova and A. C. Newell, J. Fluid Mech. **415**, 285 (2000).
[13] A. A. Golovin, S. H. Davis, and P. W. Voorhees, Phys. Rev. E **68**, 056203 (2003).
[14] W. Schöpf and L. Kramer, Phys. Rev. Lett. **66**, 2316 (1991).
[15] *Handbook of Chaos Control*, 2nd ed., edited by E. Schöll and H. G. Schuster (Wiley-VCH, Weinheim, 2008).
[16] A. S. Mikhailov and K. Showalter, Phys. Rep. **425**, 79 (2006).
[17] J. Tang and H. H. Bau, Phys. Rev. Lett. **70**, 1795 (1993).
[18] P. K. Yuen and H. H. Bau, J. Fluid Mech. **317**, 91 (1996).
[19] L. E. Howle, Phys. Fluids **9**, 1861 (1997).
[20] J. Tang and H. H. Bau, J. Fluid Mech. **363**, 153 (1998).
[21] H. H. Bau, Int. J. Heat Mass Transfer **42**, 1327 (1999).
[22] A. C. Or and R. E. Kelly, J. Fluid Mech. **440**, 27 (2001).
[23] R. O. Grigoriev, Phys. Fluids **14**, 1895 (2002).
[24] R. O. Grigoriev, Phys. Fluids **15**, 1363 (2003).
[25] P. A. Monkewitz, E. Berger, and M. Schumm, Eur. J. Mech. B Fluids **10**, 295 (1991).
[26] D. S. Park, D. M. Ladd, and E. W. Hendriks, Phys. Lett. A **182**, 244 (1993).
[27] E. Lauga and T. R. Bewley, J. Fluid Mech. **512**, 343 (2004).
[28] T. Sakurai, E. Mihaliuk, F. Chirila, and K. Showalter, Science **296**, 2009 (2002).
[29] E. Mihaliuk, T. Sakurai, F. Chirila, and K. Showalter, Phys. Rev. E **65**, 065602(R) (2002).
[30] V. K. Vanag, A. M. Zhabotinsky, and I. R. Epstein, J. Phys. Chem. A **104**, 11566 (2000).
[31] I. R. Epstein, ACS Symp. Ser. **827**, 103 (2002).
[32] D. Lebiedz and U. Brandt-Pollmann, Phys. Rev. Lett. **91**, 208301 (2003).
[33] M. Bertram and A. S. Mikhailov, Phys. Rev. E **63**, 066102 (2001).
[34] M. Bertram and A. S. Mikhailov, Phys. Rev. E **67**, 036207 (2003).
[35] C. Beta, M. Bertram, A. S. Mikhailov, H. H. Rotermund, and G. Ertl, Phys. Rev. E **67**, 046224 (2003).
[36] R. Martin, A. J. Scroggie, G.-L. Oppo, and W. J. Firth, Phys. Rev. Lett. **77**, 4007 (1996).
[37] A. V. Mamaev and M. Saffman, Phys. Rev. Lett. **80**, 3499 (1998).
[38] T. V. Savina, A. A. Nepomnyashchy, S. Brandon, D. R. Lewin, and A. A. Golovin, J. Cryst. Growth **240**, 292 (2002).
[39] A. A. Nepomnyashchy, A. A. Golovin, V. Gubareva, and V. Panfilov, Physica D **199**, 61 (2004).
[40] D. Battogtokh and A. Mikhailov, Physica D **90**, 84 (1996).
[41] D. Battogtokh, A. Preusser, and A. Mikhailov, Physica D **106**, 327 (1997).
[42] Y. Kawamura and Y. Kuramoto, Phys. Rev. E **69**, 016202 (2004).
[43] K. A. Montgomery and M. Silber, Nonlinearity **17**, 2225 (2004).
[44] C. M. Postlethwaite and M. Silber, Physica D **236**, 65 (2007).
[45] B. Y. Rubinstein, A. A. Nepomnyashchy, and A. A. Golovin, Phys. Rev. E **75**, 046213 (2007).
[46] A. A. Golovin and A. A. Nepomnyashchy, Phys. Rev. E **73**, 046212 (2006).
[47] L. G. Stanton and A. A. Golovin, Phys. Rev. E **76**, 036210 (2007).
[48] J. D. Murray, *Mathematical Biology* (Springer-Verlag, Berlin, 1989).
[49] G. Röder, G. Bordyugov, H. Engel, and M. Falcke, Phys. Rev. E **75**, 036202 (2007).
[50] K. Pyragas, Phys. Lett. A **170**, 421 (1992).
[51] M. Dahlem, F. M. Schneider, and E. Schöll, Chaos **18**, 026110 (2008).